Contribution from the Institut für Anorganische, Analytische und Physikalische Chemie der Universität Bern, CH-3000 Bern 9, Switzerland

Superexchange in Bis(μ-hydroxo)-Bridged Chromium(III) Dimers. Optical Spectroscopic Study of Singly Excited $^2E_g{}^4A_{2g}$ Pair States

SILVIO DECURTINS[1] and HANS U. GÜDEL*

Received February 25, 1982

The compounds $[(en)_2Cr(OH)_2Cr(en)_2]Br_4\cdot 2H_2O$ (abbreviated $[en]Br_4\cdot 2H_2O$), $[(NH_3)_4Cr(OH)_2Cr(NH_3)_4]Cl_4\cdot 4H_2O$ (abbreviated $[NH_3]Cl_4\cdot 4H_2O$), and $[(NH_3)_4Cr(OH)_2Cr(NH_3)_4]Br_4\cdot 4H_2O$ (abbreviated $[NH_3]Br_4\cdot 4H_2O$) have been investigated by single-crystal absorption spectroscopy in the region of $^4A_{2g}{}^4A_{2g} \rightarrow {}^2E_g{}^4A_{2g}$ pair excitations. The exchange splitting in the ground and excited states was elucidated and rationalized in terms of the nine orbital parameters $J_{ai\,bj}$. Superexchange through the bridging hydroxo ligand is by far the most important mechanism. Direct exchange plays a minor part. With the coordinate system of Figure 1 the following parameters were obtained (in cm^{-1}, with an estimated error of 20%): $J_{ab,g} = -15$, $J_{yz\,zx} = -145$, $J_{xy\,xy} = -5$, $J_{yz\,yz} = 33$, $J_{yz\,xy} = 22$, for $[en]Br_4\cdot 2H_2O$; $J_{ab,g} = -0.63$, $J_{yz\,zx} = -65$, $J_{xy\,xy} = -8$, $J_{yz\,yz} = 25$, $J_{yz\,xy} = 20$ for $[NH_3]Cl_4\cdot 4H_2O$; $J_{ab,g} = -0.3$, $J_{yz\,zx} = -55$, $J_{xy\,xy} = -8$, $J_{yz\,yz} = 17$, $J_{yz\,xy} = 20$ for $[NH_3]Br_4\cdot 4H_2O$. Hydrogen bonding of the bridging OH group to Cl and Br is responsible for the drastic reduction of $J_{yz\,zx}$ and thus J_{ab} in the $[NH_3]$ salts. Some of the spectroscopic transitions in $[NH_3]Cl_4\cdot 4H_2O$ are extremely sharp (less than 1 cm^{-1}) and zero-field splittings in the excited pair states due to single-ion anisotropies are well resolved. They can be reproduced by the spin Hamiltonian parameters $D_e = 1.3$ cm^{-1} and $E_e = -0.2$ cm^{-1}. Both pair and single-ion mechanisms contribute to the intensities of the pair transitions.

1. Introduction

The structural and magnetic properties of a large number of bis(μ-hydroxo)-bridged dimeric chromium(III) complexes have been investigated in recent years.[2a] Unlike the analogous copper(II) complexes[2b] the chromium(III) dimers do not exhibit a clear-cut correlation between the bridging geometry and the magnitude of the ground-state exchange parameter $J_{ab,g}$ (defined in eq 1).[3,4] No correlation whatever was found between the singlet-triplet separation (ranging from 0 to 54 cm^{-1}) and the Cr-Cr distance (ranging from 2.95 to 3.06 Å). Great variations of singlet-triplet splittings were observed for the same complex, $[(en)_2Cr(OH)_2Cr(en)_2]^{4+}$ (en = ethylenediamine), in different crystal environments.[3] This can be understood if external factors such as hydrogen bonding of the hydroxo group to neighboring anions or molecules in the crystal have an appreciable effect on the intramolecular exchange coupling.[5,6] This implies that superexchange is the dominant mechanism and that the direct exchange plays a minor part.

The opposite conclusion was reached for bis(μ-oxo)-bridged chromium(III) dimers obtained by doping chromium into the spinel lattices $ZnGa_2O_4$ and $MgAl_2O_4$.[7,8] On the basis of optical spectroscopic studies a dominant direct-exchange mechanism was postulated. Another piece of evidence that was interpreted in support of a dominant direct exchange is a correlation of asymptotic Curie temperatures Θ_C with Cr-Cr distances in a number of antiferromagnetic chromium(III) oxides containing a bis(μ-oxo) structural unit.[9] The nearest-neighbor distances in these oxides are comparable to the shortest Cr-Cr separations in the diol complexes, and it is difficult to see why the direct-exchange mechanism should be much stronger in the former. We therefore decided to investigate this question by a detailed optical spectroscopic study of three salts of chromium(III) diol complexes with vastly different exchange splittings in the ground state.

The ground-state splitting in a chromium(III) dimer can to a good approximation be described by a Heisenberg Hamiltonian:

$$H_{ex,g} = -2J_{ab,g}(\vec{S}_a\cdot\vec{S}_b) \quad (1)$$

In terms of an orbital model the exchange parameter J_{ab} can be expressed as an average of nine orbital parameters, $J_{ai\,bj}$, where i and j number the singly occupied t_{2g} orbitals. No insight into the orbital mechanisms, i.e., the relative magnitude of the various $J_{ai\,bj}$ contributions to the total J_{ab}, is therefore obtained from a study of the ground-state properties. An analysis of excited pair states, on the other hand, may provide this information. Singly excited pair states $^2E_g{}^4A_{2g}$ have been studied in a variety of dimers by absorption and luminescence spectroscopy.[7,8,10-15] Most of the studies have been done on transparent host crystals doped with small amounts of chromium(III), e.g., Al_2O_3,[12] $LaAlO_3$,[13] $YAlO_3$[14] $ZnGa_2O_4$,[7] $MgAl_2O_4$,[8] and MgO.[15] The advantage of these systems is their high symmetry and the resulting high symmetry of the pairs. The main disadvantage lies in the fact that there is always more than one chromophoric species present in the crystal. Besides the pairs there are single ions, triples, etc. More than one type of pair may contribute to the spectrum, as in ruby, where lines from at least four different pairs have been identified in the spectrum. The difficulties arising from this situation may be partly overcome by the use of elaborate techniques like time-resolved spectroscopy and selective-site spectroscopy.[16] In the case of chromium(III) dimers nature provides a great variety of "natural" complexes, which are free of the above-mentioned difficulties. They usually crystallize in low-symmetry crystal systems, which is normally considered to be a disadvantage for optical spectroscopy. In the present study of three triclinic chromium(III) diol complexes we can make good use of the fact that there is only one molecule per unit cell. Exchange mechanisms are elucidated by a full analysis of singly excited $^2E_g{}^4A_{2g}$ pair states. The compounds

(1) Present address: Department of Chemistry, Oregon State University, Corvallis, OR 97331.
(2) (a) Larsen, S.; Hansen, B. *Acta Chem. Scand., Ser. A* **1981**, *A35*, 105 and ref 1-9 therein. (b) Hodgson, D. J. *Prog. Inorg. Chem.* **1975**, *19*, 173.
(3) Scaringe, R. P.; Hatfield, W. E.; Hodgson, D. J. *Inorg. Chem.* **1977**, *16*, 1600.
(4) Beutler, A.; Güdel, H. U.; Snellgrove, T. R.; Chapuis, G.; Schenk, K. *J. Chem. Soc., Dalton Trans.* **1979**, 983.
(5) Michelsen, K.; Pedersen, E. *Acta Chem. Scand., Ser. A* **1978**, *A32*, 847.
(6) Decurtins, S.; Güdel, H. U.; Pfeuti, A. *Inorg. Chem.* **1982**, *21*, 1101.
(7) van Gorkom, G. G. P.; Henning, J. C. M.; van Stapele, R. P. *Phys. Rev. B: Solid State* **1973**, *8*, 955.
(8) van den Boom, H.; Van Dijsseldonk, A. J. J.; Henning, J. C. M. *J. Chem. Phys.* **1977**, *66*, 2368.
(9) Motida, K.; Miyahara, S. *J. Phys. Soc. Jpn.* **1970**, *28*, 1188; **1970**, *29*, 516.
(10) Dubicki, L. *Aust. J. Chem.* **1972**, *25*, 739.
(11) Ferguson, J.; Güdel, H. U. *Aust. J. Chem.* **1973**, *26*, 505.
(12) Ferguson, J.; van Oosterhout, B. *Solid State Commun.* **1978** *27*, 1241 and ref 1-5 therein.
(13) van der Ziel, J. P. *Phys. Rev. B: Solid State* **1971**, *4*, 2888.
(14) van der Ziel, J. P. *J. Chem. Phys.* **1972**, *57*, 2442.
(15) Imbusch, G. F.; Schawlow, A. L.; May, A. D.; Sugano, S. *Phys. Rev.* **1965**, *140*, A830.
(16) Mollenauer, L. F.; Schawlow, A. L. *Phys. Rev.* **1968**, *168*, 309.

0020-1669/82/1321-3598$01.25/0

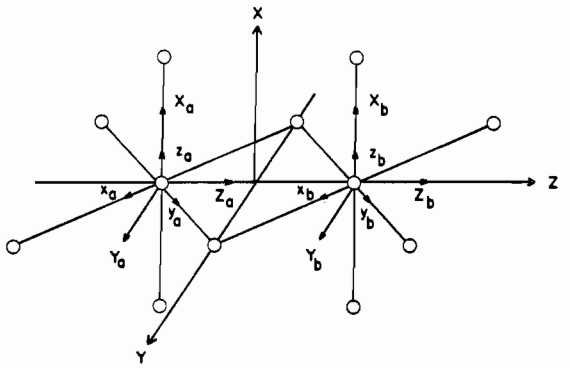

Figure 1. Coordinate systems used for $[(en)_2Cr(OH)_2Cr(en)_2]^{4+}$ and $[(NH_3)_4Cr(OH)_2Cr(NH_3)_4]^{4+}$ assuming idealized D_{2h} and C_{2v} symmetry for the pair and single ion, respectively.

studied are $[(en)_2Cr(OH)_2Cr(en)_2]Br_4 \cdot 2H_2O$ (abbreviated $[en]Br_4 \cdot 2H_2O$ in the following), $[(NH_3)_4Cr(OH)_2Cr(NH_3)_4]Cl_4 \cdot 4H_2O$ (abbreviated $[NH_3]Cl_4 \cdot 4H_2O$) and $[(NH_3)_4Cr(OH)_2Cr(NH_3)_4]Br_4 \cdot 4H_2O$ (abbreviated $[NH_3]Br_4 \cdot 4H_2O$).

2. Experimental Section

The preparation of the compounds under investigation has been described together with their structural and optical characterization.[6] They all crystallize in the triclinic system with one dimeric complex per unit cell.[4,6] All the molecules are thus parallel in the crystal. Crystal extinction directions show no measurable dispersion in the wavelength range studied here. In the projections of interest molecular symmetry axes nearly coincide with the extinction directions. Spectra measured with the electric vector parallel to the extinction directions can therefore be interpreted in terms of molecular symmetry without any transformation.[6]

2.1. Spectroscopic Measurements. Three different experimental setups were used for the measurement of polarized single-crystal absorption spectra.

Survey spectra in the temperature range 6–300 K were recorded on a Cary 17 equipped with a red-sensitive GaAs photocathode with use of a helium gas flow technique for cooling and a matched pair of Glan-Taylor prisms for polarization. For the measurement of the smallest crystals (edge lengths 0.01 mm × 0.2 mm × 0.2 mm) condensing optics consisting of a pair of Ealing-Beck reflecting objectives were introduced into the sample beam.[17]

Since some of the absorption bands had widths of less than 1 cm^{-1}, the resolving power of the Cary 17 was not sufficient. A 1402 Spex double monochromator was then used to disperse the light of a xenon arc lamp. A double-beam attachment, which was built in this laboratory, was used for the absorption measurements. The light was detected with a cooled RCA 31034 PM tube. The temperature range (flow-tube cooling technique) was 6–300 K.

Ground-state splittings of the order of 1 cm^{-1} in some of the compounds investigated resulted in very strong temperature dependencies of the spectroscopic properties below 6 K. An Oxford Instruments Spectromag 4 cryostat was used in conjunction with a $^3/_4$ m Spex monochromator for single-beam transmission measurements between 1.4 and 10 K.

For the luminescence experiments the sample was excited by the 514-nm line of an argon ion laser. The luminescence was dispersed by a 1402 Spex double monochromator and detected by a cooled RCA 31034 PM tube with use of a photon-counting technique.

3. Theory

The exact point symmetry of the dimeric complexes is C_i.[4,6] D_{2h} is an approximation, and our discussion is based on this idealized symmetry. Figure 1 shows the coordinate systems used. x_a, y_a, z_a and x_b, y_b, z_b define the local cubic coordinates. X_a, Y_a, Z_a and X_b, Y_b, Z_b define the local C_{2v} coordinate frame. X, Y, and Z are the dimer coordinates.

3.1. $^2E_g{}^4A_{2g}$ Pair States and Exchange Splittings. Both $^4A_{2g}$ and ^2E_g single-ion states derive from the $(t_{2g})^3$ electron configuration. Isotropic bilinear exchange in the singly excited $^2E_g{}^4A_{2g}$ states may therefore be described by the Hamiltonian[7,10,13]

$$H_{ex,e} = -2\sum_{i,j} J_{ai\,bj}\vec{s}_{ai}\cdot\vec{s}_{bj} \tag{2}$$

where i and j number the singly occupied t_{2g} orbitals, which are defined in the x, y, z frames in Figure 1. We number the t_{2g} orbitals as

$$1 \approx yz \qquad 2 \approx zx \qquad 3 \approx xy \tag{3}$$

The nine orbital-exchange parameters $J_{ai\,bj}$ are reduced to four by the pair symmetry:

$$J_{11} = J_{22} \qquad J_{12} = J_{21} \qquad J_{13} = J_{31} = J_{23} = J_{32} \qquad J_{33} \tag{4}$$

In the local C_{2v} site symmetry the ^2E_g single ion state is split in first order into the components $^2A_1$ (designated E_a) and $^2B_2$ (E_b). This splitting is of the order of 10–100 cm^{-1} and results in a corresponding displacement of pair states derived from E_a and E_b, respectively.

The excited-state exchange parameters are related to the orbital parameters as shown in eq 5–7.[18] Symmetries in D_{2h} and energies of the eight pair states deriving from the singly excited $^2E_g{}^4A_{2g}$ configuration are listed in Table I.

$$J_{ab}(E_a) = \tfrac{1}{3}\sum_j J_{3j} \tag{5}$$

$$J_{ab}(E_b) = \tfrac{2}{9}\sum_j (J_{1j} + J_{2j} - \tfrac{1}{2}J_{3j}) \tag{6}$$

$$J_{ab,g} = J_{ab,e} = \tfrac{1}{2}[J_{ab}(E_a) + J_{ab}(E_b)] \tag{7}$$

In eq 1 and 2 higher order terms corresponding to isotropic biquadratic as well as anisotropic interactions have been neglected. A satisfactory analysis of experimental energy splittings was possible without the inclusion of such terms. Deviations from predicted selection rules and intensity ratios, on the other hand, may be the result of some anisotropy in their pair states.

3.2. Zero-Field Splittings in $^2E_g{}^4A_{2g}$ Pair States. The pair states are split in second order by the combined action of the low-symmetry ligand field and spin–orbit coupling. This zero-field splitting is of the order of 1–5 cm^{-1}. It is usually unresolved in the optical spectra of chromium(III) pairs, and it has so far been neglected. Pair transitions of $[NH_3]Cl_4 \cdot 4H_2O$ and $[NH_3]Br_4 \cdot 4H_2O$ are extremely narrow, and the fine structure resulting from excited-state zero-field splittings are well resolved for a number of transitions. The splitting can be represented by the spin Hamiltonian

$$H_{Zf} = D[S_{Z_a}{}^2 + S_{Z_b}{}^2 - \tfrac{5}{2}] + E(S_{X_a}{}^2 + S_{X_b}{}^2 - S_{Y_a}{}^2 - S_{Y_b}{}^2) \tag{8}$$

Table I. Symmetries in D_{2h} and Energy Eigenvalues of Pair States[a]

pair states	$^2E_g{}^4A_{2g}$ energies
$^3B_{2u}$	$-^1/_3J_{12} + ^1/_3J_{11} + ^5/_6J_{33} + ^5/_3J_{13} + R_a$
$^3B_{3g}$	$+^1/_3J_{12} - ^1/_3J_{11} + ^5/_6J_{33} + ^5/_3J_{13} + R_a$
$^3B_{1u}$	$+^{11}/_9J_{12} + ^{11}/_9J_{11} - ^1/_{18}J_{33} + ^1/_9J_{13} + R_b$
^3A_g	$J_{12} + J_{11} - ^1/_2J_{33} + J_{13} + R_b$
$^5B_{2u}$	$J_{12} - J_{11} - ^1/_2J_{33} - J_{13} + R_a$
$^5B_{3g}$	$-J_{12} + J_{11} - ^1/_2J_{33} - J_{13} + R_a$
$^5B_{1u}$	$-J_{12} - J_{11} - ^1/_2J_{33} + J_{13} + R_b$
^5A_g	$-^1/_3J_{12} - ^1/_3J_{11} + ^5/_6J_{33} - ^5/_3J_{13} + R_b$

[a] R_a and R_b are energies of E_a and E_b single-ion transitions, respectively.

(17) Ferguson, J.; Orr, W. *Rev. Sci. Instrum.* **1973**, *44*, 225.

(18) Ferguson, J.; Guggenheim, H. J.; Tanabe, Y. *J. Phys. Soc. Jpn.* **1966**, *21*, 692.

Table II. Matrix of the Operator (8) in the Basis $|SM_S\pm\rangle = (1/2^{1/2})(|SM_S\rangle \pm |S-M_S\rangle)$ for Singly Excited $^2E_g{}^4A_{2g}$ Pair States[a]

$^3\Gamma$	$\|11+\rangle$	$\|11-\rangle$	$\|10\rangle$
$\langle 11+\|$	$+^1/_2D$ $+^3/_2E$	0	0
$\langle 11-\|$	0	$+^1/_2D$ $-^3/_2E$	0
$\langle 10\|$	0	0	$-D$

$^5\Gamma$	$\|22+\rangle$	$\|22-\rangle$	$\|21+\rangle$	$\|21-\rangle$	$\|20\rangle$
$\langle 22+\|$	$+D$	0	0	0	$3^{1/2}E$
$\langle 22-\|$	0	$+D$	0	0	0
$\langle 21+\|$	0	0	$-^1/_2D$ $+^3/_2E$	0	0
$\langle 21-\|$	0	0	0	$-^1/_2D$ $-^3/_2E$	0
$\langle 20\|$	$3^{1/2}E$	0	0	0	$-D$

[a] The matrix is independent of Γ.

D and E are axial and rhombic anisotropy parameters, defined in the local C_{2v} coordinate frame, and $S_a = S_b = {}^3/_2$. The parameters should be the same for all the pair states deriving from a given excited configuration. Table II lists the matrices of (8) in a $|\Gamma SM_S\pm\rangle = (1/2^{1/2})(|\Gamma SM_S\rangle \pm |\Gamma S-M_S\rangle)$ basis for the singly excited $^2E_g{}^4A_{2g}$ pair states. The matrices are independent of Γ.

3.3. Intensity Mechanisms. There are two well-established mechanisms by which spin-forbidden transitions can acquire intensity in an exchange-coupled pair of ions:[19] (1) a single-ion mechanism, which is based on the odd-parity crystal field in conjunction with spin–orbit coupling; (2) a pair mechanism, which has its origin in the exchange coupling. Our spectra provide clear evidence of both these mechanisms. On the other hand, there are a number of features, e.g., the appearance of absorption bands with $\Delta S = 2$, which can be rationalized by neither of them and which, therefore, must have their origins in alternative mechanisms.

3.3.1. Single-Ion Mechanism. The $^4A_{2g} \rightarrow {}^4T_{2g}$, $^4T_{1g}$ single-ion transitions obtain their intensity through the odd-parity crystal-field potential V_u at the chromium(III) centers. They can, in turn, act as a source of intensity for the $^4A_{2g} \rightarrow {}^2E_g$ transitions through a spin–orbit coupling mechanism:[20]

$$^4A_{2g} \xrightarrow{V_u\cdot\vec{P}} {}^4\Gamma_g \xrightarrow{H_{so}} {}^2E_g \qquad (9)$$

$\vec{P}$ is the electric dipole moment.

The effective transition moment of the spin-allowed transition can be written[21]

$$\vec{P}_{eff}(^4A_{2g} \rightarrow {}^4\Gamma_g) = \sum_I \frac{\langle {}^4\Gamma_g|V_u|I\rangle\langle I|\vec{P}|{}^4A_{2g}\rangle}{E(^4\Gamma_g) - E(I)} + \sum_I \frac{\langle {}^4\Gamma_g|\vec{P}|I\rangle\langle I|V_u|{}^4A_{2g}\rangle}{E(^4A_{2g}) - E(I)} \qquad (10)$$

where the sum includes all the odd-parity states $|I\rangle$. The most likely states $|I\rangle$ are those arising from a ligand to metal electron transfer. It can be shown that the lowest energy charge-transfer states arising from $t_u \rightarrow t_{2g}$ excitations only provide minor contributions to the $^4A_{2g} \rightarrow {}^4T_{2g}$, $^4T_{1g}$ intensity.[6] X-polarized $t_u \rightarrow e_g$ excitations dominate, and as a consequence, $\vec{P}_{eff}(^4A_{2g} \rightarrow {}^4T_g)$ has a dominant X component. This is in good agreement with the observed dichroic ratios: both $^4A_{2g} \rightarrow {}^4T_{2g}$ and $^4A_{2g} \rightarrow {}^4T_{1g}$ transitions are approximately one order of magnitude more intense in X polarization than in Y and Z.[6]

Table III. Nonvanishing Transformation Matrix Elements $\langle\Gamma\gamma|\Gamma M\rangle$[a]

$\langle E_u|E_a\rangle = \langle E_v|E_b\rangle = 1$
$\langle T_{1z}|T_1X\rangle = \langle T_{2\xi}|T_{2\alpha}\rangle = 1$
$\langle T_{1x}|T_1Y\rangle = \langle T_{1y}|T_1X\rangle = \langle T_{1y}|T_1Z\rangle = -\langle T_{1x}|T_1Z\rangle = 1/2^{1/2}$
$\langle T_{2\eta}|T_{2\gamma}\rangle = \langle T_{2\xi}|T_{2\gamma}\rangle = \langle T_{2\xi}|T_{2\beta}\rangle = -\langle T_{2\eta}|T_{2\beta}\rangle = 1/2^{1/2}$

[a] $|\Gamma\gamma\rangle$ and $|\Gamma M\rangle$ refer to the x, y, z and X, Y, Z coordinate systems in Figure 1, respectively. The transformations are independent of parity.

Table IV. Expansion of $V_{\bar{\gamma}}(\bar{\Gamma})\cdot P_{\gamma'}(\Gamma') = \Sigma_{\gamma,\Gamma} W_\gamma(\Gamma)\langle\Gamma\gamma|\Gamma'\gamma'\bar{\Gamma}\bar{\gamma}\rangle$ in the X, Y, Z Coordinate Frame[a]

$V_Z(T_{1u})\cdot P_X(T_{1u}) = -(1/2^{1/2})W_Y(T_{1g}) - (1/2^{1/2})W_\beta(T_{2g})$
$V_\gamma(T_{2u})\cdot P_X(T_{1u}) = (1/2^{1/2})W_Y(T_{1g}) + (1/2^{1/2})W_\beta(T_{2g})$
$V_Z(T_{1u})\cdot P_Y(T_{1u}) = (1/2^{1/2})W_b(E_g) + (1/2^{1/2})W_X(T_{1g})$
$V_\gamma(T_{2u})\cdot P_Y(T_{1u}) = -(1/3^{1/2})W_{e_2}(A_{2g}) - (1/6^{1/2})W_b(E_g) + (1/2^{1/2})W_X(T_{1g})$
$V_Z(T_{1u})\cdot P_Z(T_{1u}) = -(1/3^{1/2})W_{e_1}(A_{1g}) + (1/6^{1/2})W_a(E_g) + (1/2^{1/2})W_\alpha(T_{2g})$
$V_\gamma(T_{2u})\cdot P_Z(T_{1u}) = (1/2^{1/2})W_a(E_g) + (1/2^{1/2})W_\alpha(T_{2g})$

[a] Phase conventions are according to ref 21.

Equation 10 can be simplified by applying the closure approximation[21] to

$$\vec{P}_{eff}(^4A_{2g} \rightarrow {}^4\Gamma_g) = (2/\Delta E)\langle {}^4\Gamma_g|V_u\cdot\vec{P}|{}^4A_{2g}\rangle \qquad (11)$$

where ΔE is an average of energy differences $E(^4\Gamma_g) - E(I)$ and $E(^4A_{2g}) - E(I)$.

The operators in eq 11 can be considered as tensor operators. The first-order term of the C_{2v} odd-parity potential transforms as $V_\gamma(T_{1u})$ and the two third-order terms as $V_Z(T_{1u})$ and $V_\gamma(T_{2u})$. $\vec{P}$ is represented by the components $P_X(T_{1u})$, $P_Y(T_{1u})$, and $P_Z(T_{1u})$. The products of two tensor operators $V_u\cdot P$ in eq 11 can be expanded in terms of tensor operators $W_\gamma(\Gamma)$ as[21]

$$V_{\bar{\gamma}}(\bar{\Gamma})\cdot P_{\gamma'}(\Gamma') = \sum_{\gamma,\Gamma} W_\gamma(\Gamma)\langle\Gamma\gamma|\Gamma'\gamma'\bar{\Gamma}\bar{\gamma}\rangle \qquad (12)$$

where $\langle\Gamma\gamma|\Gamma'\gamma'\bar{\Gamma}\bar{\gamma}\rangle$ are the coupling coefficients in the C_{2v} coordinate system. Using the tabulated cubic coupling coefficients[21] and the transformation relations in Table III, we obtain the results in Table IV. For the spin-allowed transitions the following selection rules are immediately derived:

$$\begin{aligned} ^4A_{2g} &\rightarrow {}^4T_{2g\gamma}, {}^4T_{1gZ} \quad X \text{ polarized} \\ &\rightarrow {}^4T_{2g\alpha} \quad Y \text{ polarized} \\ &\rightarrow {}^4T_{1gX} \quad Z \text{ polarized} \end{aligned} \qquad (13)$$

Of these the X-polarized transitions have dominant intensities.

The next step is the derivation of selection rules for the spin-forbidden $^4A_{2g} \rightarrow {}^2E_g$ transitions. Spin-orbit coupling of ^2E_g to $^4T_{2g}$ and $^4T_{1g}$ according to eq 9 is the relevant mechanism. The components of the spin–orbit coupling operator can be shown to transform as the rotations, i.e., as $T_{1gX}(S_X)$, $T_{1gY}(S_Y)$, and $T_{1gZ}(S_Z)$.[22] With consideration of the fact that S_X and S_Y correspond to $\Delta M_S = \pm 1$ transitions and S_Z to $\Delta M_S = 0$ and with use of (13) the selection rules in Table V are easily obtained.

For the $^4A_{2g}{}^4A_{2g} \rightarrow {}^2E_g{}^4A_{2g}$ pair excitations the transition moments on the individual chromium(III) centers have to be properly combined. Using Table V and considering the fact that V_{ua} and V_{ub} have opposite orientations (Figure 1),[23] we derive the pair selection rules in Table VI. In contrast to the pair mechanism (section 3.3.2) transitions with $\Delta S = \pm 1$ are allowed in addition to $\Delta S = 0$ in the single-ion mechanism.

(19) Naito, M. *J. Phys. Soc. Jpn.* **1973**, *34*, 1491.
(20) Namba, K.; Tanabe, Y. *J. Phys. Soc. Jpn.* **1974**, *37*, 371.
(21) Sugano, S.; Tanabe, Y.; Kamimura, H. "Multiplets of Transition Metal Ions in Crystals"; Academic Press: New York, 1970; pp 139, 144, 286–288.
(22) Shinagawa, K.; Tanabe, Y. *J. Phys. Soc. Jpn.* **1971**, *30*, 1280.
(23) Dubicki, L., private communication.

Table V. Electric Dipole Selection Rules for $^4A_{2g} \rightarrow {}^2E_g$ Single-Ion Transitions[a]

	^2E_g			
	E_a		E_b	
$M_S =$ ($^4A_{2g}$)	$M_S =$ $^1/_2$	$M_S =$ $-^1/_2$	$M_S =$ $^1/_2$	$M_S =$ $-^1/_2$
$^3/_2$	Z		X, Y	
$^1/_2$	X	Z		X, Y
$-^1/_2$	Z	X	X, Y	
$-^3/_2$		Z		X, Y

[a] The $^2A_1$ and $^2B_2$ components of ^2E_g are designated E_a and E_b, respectively.

The two selection rules $\Delta S = \pm 1$ and $\Delta S = 0$ are mutually exclusive.

For those transitions that gain their intensity through a single-ion mechanism we expect a predominance in X polarization similar to that of the spin-allowed $^4A_{2g} \rightarrow {}^4T_{2g}$, $^4T_{1g}$ transitions.[6]

3.3.2. Pair Mechanism. $^4A_{2g} \rightarrow {}^2E_g$ single-ion excitations occur within the half-filled $(t_{2g})^3$ shell. For this special situation the interaction between the pair of ions and the electric vector of the radiation field can be represented by[18]

$$H' = \sum_{i,j} \vec{\Pi}_{ai\,bj} \vec{E} (\vec{s}_{ai} \vec{s}_{bj}) \tag{14}$$

where $\vec{\Pi}_{ai\,bj}$ is a vector related to $J_{ai\,bj}$ by

$$\Pi_{ai\,bj}{}^{\alpha} = \left(\frac{\partial J_{ai\,bj}}{\partial E^{\alpha}} \right)_{E \rightarrow 0} \tag{15}$$

For a pair with inversion symmetry we get immediately

$$\vec{\Pi}_{ai\,bj} = -\vec{\Pi}_{aj\,bi} \qquad \vec{\Pi}_{ai\,bi} = 0 \tag{16}$$

The spin selection rules

$$\Delta S = 0 \qquad \Delta M_S = 0 \tag{17}$$

apply for this mechanism. The four symmetry-allowed pair transitions and their polarizations are thus

$$^3B_{1u} \rightarrow {}^3B_{3g}(Y), {}^3A_g(Z) \qquad {}^5A_g \rightarrow {}^5B_{2u}(Y), {}^5B_{1u}(Z) \tag{18}$$

The calculated intensity ratio of corresponding triplet and quintet transitions is 5/9.[18]

4. Results and Analysis

Survey spectra and an analysis of the spin-allowed transitions in $[en]Br_4 \cdot 2H_2O$, $[NH_3]Cl_4 \cdot 4H_2O$, and $[NH_3]Br_4 \cdot 4H_2O$ have been published before.[6] Figure 2 shows a survey of the ^2E_g and $^2T_{1g}$ absorption regions in $[en]Br_4 \cdot 2H_2O$ and $[NH_3]Br_4 \cdot 4H_2O$. There is little similarity between the two spectra. In $[en]Br_4 \cdot 2H_2O$ the ground-state exchange parameter $J_{ab,g}$ is -15 cm^{-1},[4] whereas in $[NH_3]Br_4 \cdot 4H_2O$ its value is only -0.3 cm^{-1} (cf. Table VIII). The total spread of exchange splittings in the singly excited states is much smaller in $[NH_3]Br_4 \cdot 4H_2O$. As a result the ^2E_g and $^2T_{1g}$ manifolds are separated whereas in the $[en]Br_4 \cdot 2H_2O$ spectrum there is considerable overlap.

4.1. Transitions to $^2E_g{}^4A_{2g}$ in $[en]Br_4 \cdot 2H_2O$. An analysis of $^2E_g{}^4A_{2g}$ excitations is complicated by the overlap of $^2E_g{}^4A_{2g}$ and $^2T_{1g}{}^4A_{2g}$ pair states. Nonvanishing matrix elements of the exchange operator between $^2E_g{}^4A_{2g}$ and $^2T_{1g}{}^4A_{2g}$ can lead to energy shifts and mixing of wave functions. We therefore concentrate on the low-energy part of the spectrum, in which several bands can unambiguously be assigned to $^2E_g{}^4A_{2g}$ transitions on the basis of their polarizations and intensities. Figures 3 and 4 illustrate the polarization properties as well as the temperature dependence of the absorptions. At 6 K X-polarized intensity dominates the spectrum. This is not surprising in view of the spin-allowed $^4A_{2g} \rightarrow {}^4T_{2g}$ transition, centered at 18 500 cm^{-1}. It is also predominantly X polarized[6] and obviously acts as the main source of intensity for the $^2E_g{}^4A_{2g}$, $^2T_{1g}{}^4A_{2g}$ pair excitations at 6 K. This is a very nice illustration of a single-ion intensity mechanism (section 3.3.1) in pair transitions. At 6 K this mechanism is expected to provide the major part of the intensity, since $\Delta S = 0$ transi-

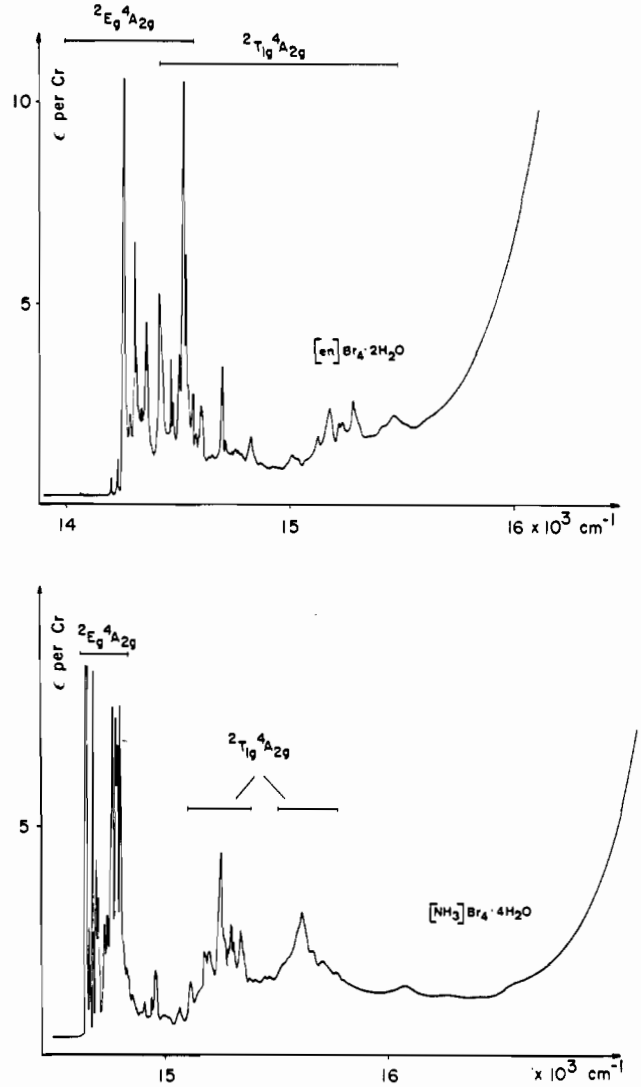

Figure 2. 6 K absorption spectra of single crystals (X polarization) of $[en]Br_4 \cdot 2H_2O$ and $[NH_3]Br_4 \cdot 4H_2O$ in the region of ^2E_g and $^2T_{1g}$ single excitations.

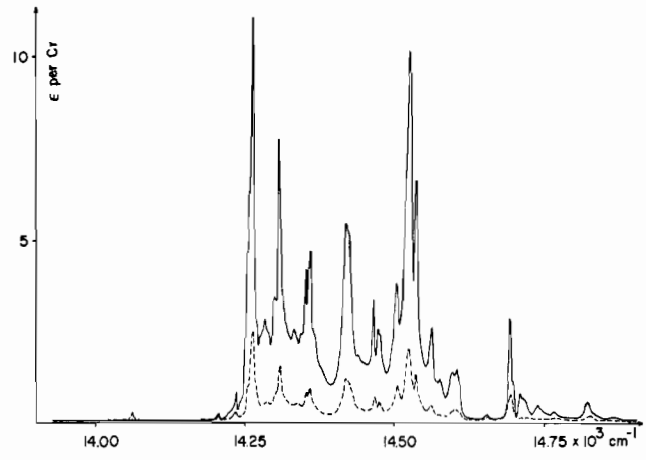

Figure 3. 6 K absorption spectra of $[en]Br_4 2H_2O$: (—) X polarization; (---) Z polarization.

Table VI. Electric Dipole Selection Rules for $^4A_{2g}{}^4A_{2g} \rightarrow {}^2E_g{}^4A_g$ Pair Transitions by a Single-Ion Intensity Mechanism[a]

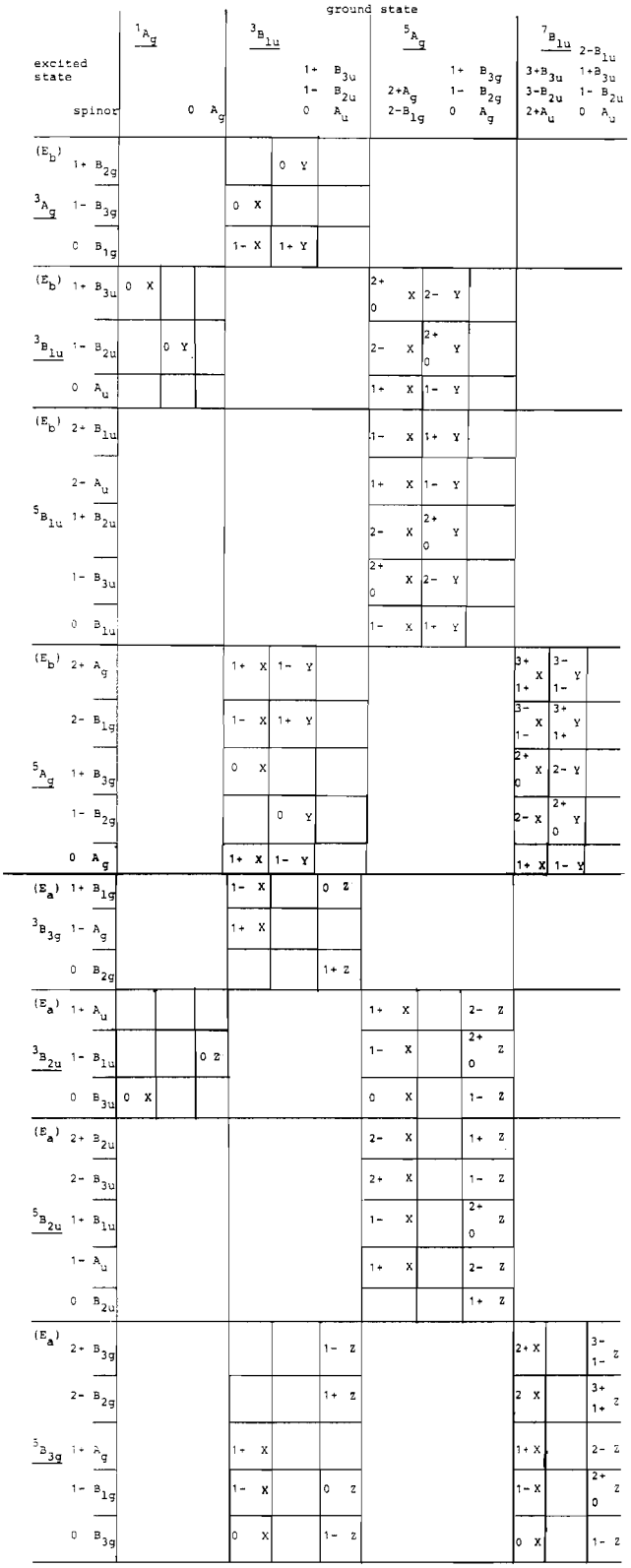

[a] The symmetry notations are in D_{2h} pair symmetry. Included are the designations $|M_S\pm\rangle = (1/2^{1/2})(|M_S\rangle \pm |-M_S\rangle)$, which form bases of the irreducible representations in the spinor group.

tions, as required by the pair mechanism, are not possible. At elevated temperatures two predominantly *Y*-polarized absorptions B_1 and A_2 appear and finally dominate the spectrum at high temperatures. The transitions are identified from their temperature dependence as originating in the $S = 1$ (B_1) and $S = 2$ (A_2) ground levels. Both transitions carry some intensity

Table VII. Band Positions (in cm^{-1}) of $^2E_g{}^4A_{2g}$ Pair Transitions in $[NH_3]Cl_4 \cdot 4H_2O$[a]

A1	14 645	+0	^5A_g
2		+1.7	^5A_g
3		+3.0	$^3B_{1u}$
4		+3.5	$^3B_{1u}$
5		+4.8	$^3B_{1u}$
6		+5.8	$^3B_{1u}$
B1	14 676	+0	^5A_g
2		+1.3	^5A_g
3		+2.1	^5A_g
4		+3.6	^1A_g
5		+5.3	^1A_g
6		+5.9	^1A_g
C1	14 693	+0	^5A_g
2		+0.9	^5A_g
3		+3.9	$^3B_{1u}$
4		+4.6	$^3B_{1u}$
5		+5.8	^1A_g
D1	14 706	+0	^5A_g
2		+0.6	^5A_g
3		+3.3	^1A_g
4		+4.0	^1A_g
E1	14 750	+0	
2		+2.2	
3		+4.3	
4		+6.6	
5		+7.0	
F1	14 782	+0	
2		+3.5	
3		+9.4	
G	14 810		
H	14 825		

[a] Pair transitions are denoted A-H, as in Figures 5, 7, and 8. Fine-structure components are numbered 1, 2, . . ., as in Figures 7 and 8. Initial states of transitions are indicated on the right-hand side.

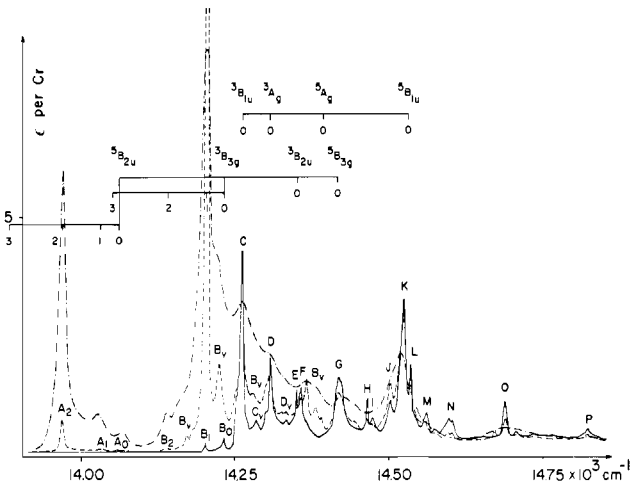

Figure 4. *Y*-polarized absorption spectra of $[en]Br_4 2H_2O$: (—) 6 K; (---) 19 K; (-·-·-) 43 K. The designation of absorption bands A, B, ... is used in the text. Bands with a subscript v are vibrational sidebands. The calculated energies were obtained with the parameters in Table VIII.

in *X* and *Z* polarization, but *Y* intensity is stronger by almost an order of magnitude. This is compatible with a dominant contribution in *Y* polarization from a pair mechanism and small contributions in *X*, *Y*, and *Z* from a single-ion mechanism. The transitions thus follow $\Delta S = 0$, and inspection of the pair selection rules (eq 18) reveals that there is only one possible assignment:

$$^3B_{1u} \rightarrow {}^3B_{3g} \text{ for } B_1 \qquad {}^5A_g \rightarrow {}^5B_{2u} \text{ for } A_2$$

Their experimental intensity ratio in *Y* polarization (corrected for Boltzmann populations) is 0.35. This compares favorably with the theoretical value of 0.56 for a pure pair mechanism.

Table VIII. Structural and Exchange Parameters[a]

compd	structure: Cr-Cr, Å	structure: Cr–O–Cr, deg	ground state $J_{ab,g}$	excited $^2E_g{}^4A_{2g}$ state: $R_a - R_b$	J_{12}	J_{33}	J_{11}	J_{13}	$J_{ab,e}$
$[en]Br_4 \cdot 2H_2O$	3.038 (4)	6 (2)[4]	−15 (1)	−140	−145	−5	33	22	−16
$[NH_3]Cl_4 \cdot 4H_2O$	2.95 (5)	>30[6,25]	−0.63 (8)	33	−65	−8	25	20	−0.9
$[NH_3]Br_4 \cdot 4H_2O$	2.95 (5)	>30[6,25]	−0.30 (15)	34	−55	−8	17	20	−0.4

[a] All J values are in cm^{-1}.

The lowest energy pair excitations can therefore be considered as pure $^4A_{2g}{}^4A_{2g} \rightarrow {}^2E_g{}^4A_{2g}$ transitions. Perturbations by the nearby $^2T_{1g}{}^4A_{2g}$ excitations are small. The 2-cm^{-1} splitting of the A_2 band is the result of zero-field splittings in the excited $^5B_{2u}$ pair state.

Of the large number of higher energy absorption bands in the 6 K spectrum only two can be assigned to allowed $^2E_g{}^4A_{2g}$ transitions according to the theory (Table VI). Some peaks are identified as vibrational sidebands of the more prominent electronic origins from a comparison with the luminescence spectrum (Figure 4). A further distinction can be made on the basis of bandwidths. The peaks A, B, C, D, E, F, H, and L are considerably narrower than the peaks G, I, J, K, M, ... Since transitions to $^2T_{1g}$ are often found to be broader than ^2E_g transitions in chromium(III) spectra, we make the tentative assumption that the first group of peaks belongs to $^2E_g{}^4A_{2g}$ excitations. There is thus considerable overlap with $^2T_{1g}{}^4A_{2g}$ pair excitations, and the resulting perturbations make a detailed analysis of the high-energy part of the spectrum impossible. Nevertheless we have a good estimate of the total spread of $^2E_g{}^4A_{2g}$ excitations. And we can confidently assign the high-intensity band C to one of the allowed transitions $^1A_{1g} \rightarrow {}^3B_{1u}$ or $^1A_{1g} \rightarrow {}^3B_{2u}$ (Table VI). This, together with the firm assignments of the bands A_2 and B_1, enables us to derive good estimates of the excited-state exchange parameters. With the plausible constraints[7,10,13]

$$J_{ab,e} \simeq J_{ab,g} \qquad J_{33} < 0,\ J_{12} < 0,\ J_{11} > 0,\ J_{13} > 0 \qquad |J_{12}| > |J_{11}| \tag{19}$$

the following set of orbital parameters is derived:

$$\left.\begin{aligned} J_{12} &= -145\ cm^{-1} \\ J_{33} &= -5\ cm^{-1} \\ J_{11} &= 33\ cm^{-1} \\ J_{13} &= 22\ cm^{-1} \end{aligned}\right\} \quad J_{ab,e} = -16\ cm^{-1} \tag{20}$$

The corresponding energy splitting is included in Figure 4. The parameters have an estimated error of ±20%.

It must be emphasized that the main result, i.e., the dominance of superexchange (J_{12}) vs. direct exchange (J_{33}), follows directly from the fact that $^5B_{2u}$ and $^3B_{3g}$ are the two lowest energy $^2E_g{}^4A_{2g}$ pair states. It is therefore independent of the remaining uncertainties in the assignments of high-energy bands. If the opposite was true, i.e., $|J_{33}| >> |J_{12}|$, the lowest energy states would be ^5A_g and $^3B_{1u}$ and the corresponding absorption bands could not have the observed predominance in Y polarization from a pair mechanism.

The selection rules derived in section 3.3 are not strictly obeyed. This follows from the fact that the 6 K spectrum contains more than two sharp electronic origins. A specific and experimentally very well documented example is the band A_0 corresponding to the $^1A_{1g} \rightarrow {}^5B_{2u}$ transition. It is particularly prominent in Z polarization (Figure 3). Neither of the two mechanisms discussed in section 3.3 can explain a $\Delta S = 2$ transition. From the observed zero-field splittings we know that there is some anisotropy in the excited pair states. This has not been considered in our theory, and it is likely to relax the spin as well as the symmetry selection rules. In addition the real single-ion site symmetry is C_i, and the selection rules derived on the basis of the idealized symmetry C_{2v} are too restrictive.

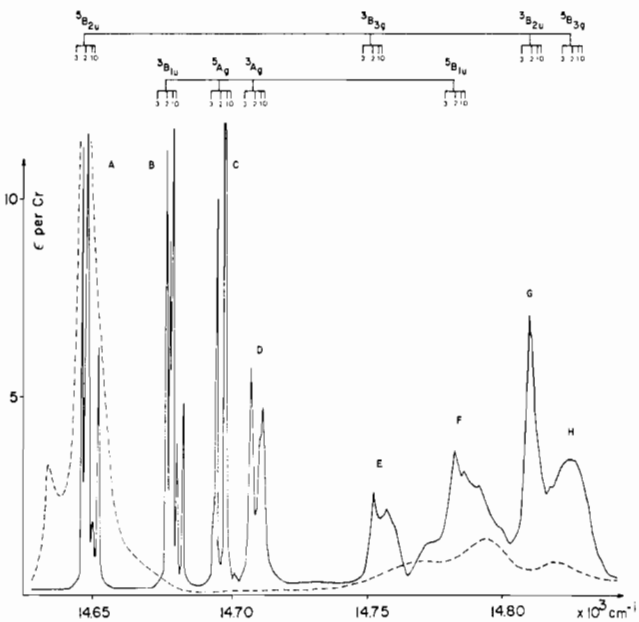

Figure 5. 9 K X-polarized absorption spectrum of $[NH_3]Cl_4 \cdot 4H_2O$ in the region of $^2E_g{}^4A_{2g}$ pair excitations. A mirror image of the (unpolarized) luminescence spectrum built on transition A is included (- - -). The calculated energies were obtained with the parameters in Table VIII.

4.2. Transitions to $^2E_g{}^4A_{2g}$ in $[NH_3]Cl_4 \cdot 4H_2O$ and $[NH_3]Br_4 \cdot 4H_2O$. Low-temperature spectra in the region of lowest energy absorptions are shown in Figures 5 and 6. Compared with the case for $[en]Br_4 \cdot 4H_2O$ the total spread is reduced by a factor of 3–4. The main changes of intensity with temperature occur below 4.2 K. This is the result of the very small exchange splittings in the ground state, and it can be used (vide infra) for a quantitative estimate of the corresponding parameters. Some bands in the bromide spectrum can be identified as vibronic sidebands from a comparison with the luminescence spectrum. They are identified as such in Figure 6.

The lowest energy transitions in the chloride spectrum consist of several well-resolved components. Line widths are less than 1 cm^{-1}. With increasing energy the bands lose their sharpness. We interpret this broadening as the result of an interaction between vibronic and coinciding electronic transitions. As illustrated in Figure 5 there is a first very weak sideband of A coinciding with D, and several stronger sidebands of A–D fall into the E–H region. Figures 7 and 8 provide an illustration of the richness of the fine structure in the bands A–C and of the polarization effects observed. None of the chromium(III) pair systems reported so far in the literature shows us much fine structure of absorption bands.

The fine structure is the result of exchange splittings in the ground state and zero-field splittings in the excited states as illustrated schematically in Figure 9 for the transition B. The two effects can be separated from the temperature dependence of intensities. Figure 10 shows transmission spectra of [N-

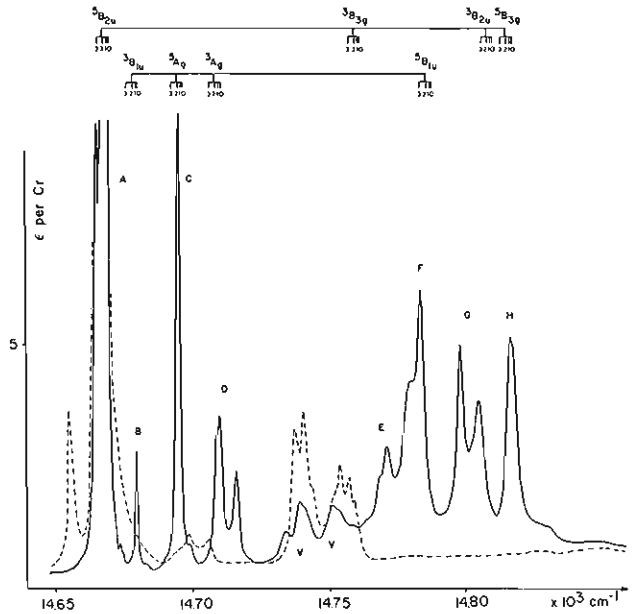

Figure 6. Absorption and luminescence spectra of $[NH_3]Br_4 \cdot 4H_2O$ as for Figure 5. Vibrational sidebands in the absorption spectrum are denoted by a subscript v.

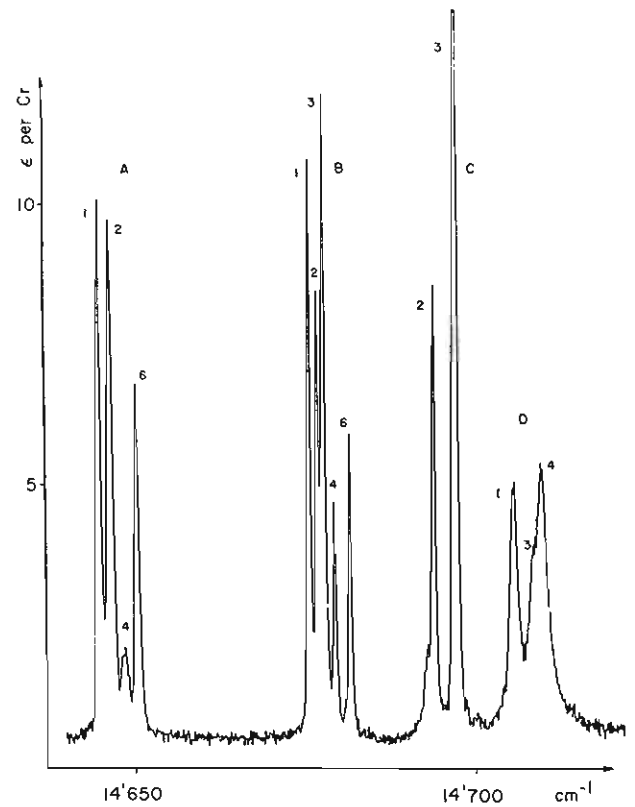

Figure 7. High-resolution absorption spectra of the four lowest energy pair excitations A, B, C, and D in $[NH_3]Cl_4 \cdot 4H_2O$, with $T = 6$ K and X polarization. The numbering of fine-structure components is the same as in Table VII. It is used in the text.

$H_3]Cl \cdot 4H_2O$ between 4.2 and 1.4 K. The observed temperature dependences are in good overall agreement with those calculated for a ground-state splitting pattern with $J_{ab,g} = -0.6$ cm^{-1} (Figure 11). Band positions and initial states of the transitions are collected in Table VII. Transition B strictly obeys a $\Delta S = \pm 1$ selection rule (Figure 9), and it is therefore particularly easy to determine both ground- and excited-state splittings.

The energy differences B4–B1 (3.6 cm^{-1}), B5–B2 (4.0 cm^{-1}), and B6–B3 (3.8 cm^{-1}) are a measure of the energy difference

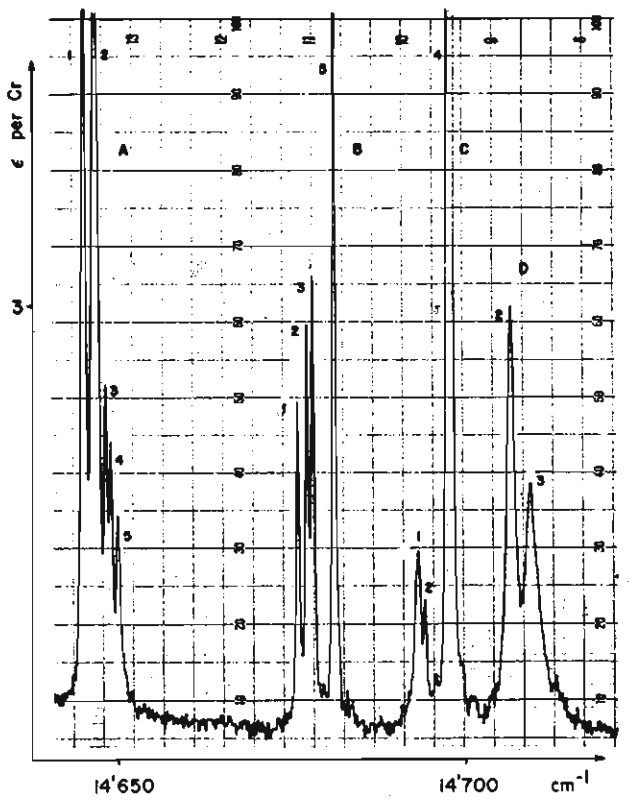

Figure 8. Absorption spectrum as for Figure 7, but with Z polarization.

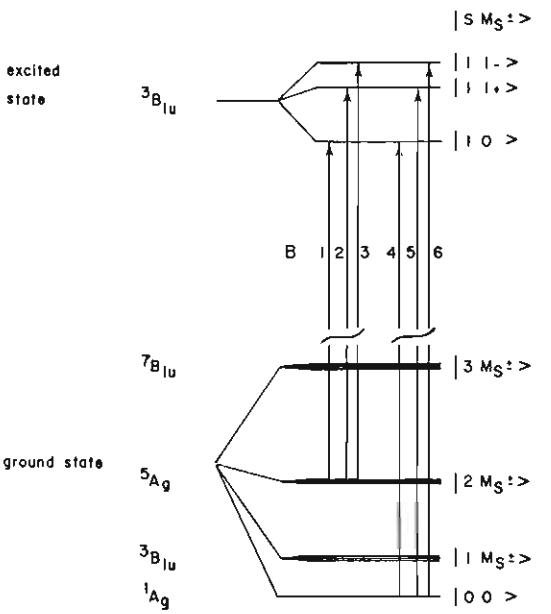

Figure 9. Schematic representation of ground- and excited-state splittings leading to the fine structure of band system B. $|SM_S\pm) = (1/2^{1/2})(|SM_S\rangle \pm |S - M_S\rangle)$.

^5A_g–^1A_g in the ground state. Assuming a Landé type exchange splitting pattern (eq 1), we obtain $J_{ab,g} = -0.63 \bullet 0.08$ cm^{-1}. We also obtain an estimate of the zero-field splitting of the ^5A_g ground level. It is 0.2–0.3 cm^{-1}, corresponding to anisotropy parameters of the order of 0.1 cm^{-1}. This effect is one order of magnitude smaller than in the excited pair states (next paragraph) and in good agreement with theoretical expectations.

The energy differences within the set B4, B5, B6 (0, 1.7, 2.3 cm^{-1}) define the zero-field splitting of the excited pair state. It can be reproduced by the spin Hamiltonian parameters

$$D = 1.3 \text{ cm}^{-1} \qquad E = -0.2 \text{ cm}^{-1} \qquad (21)$$

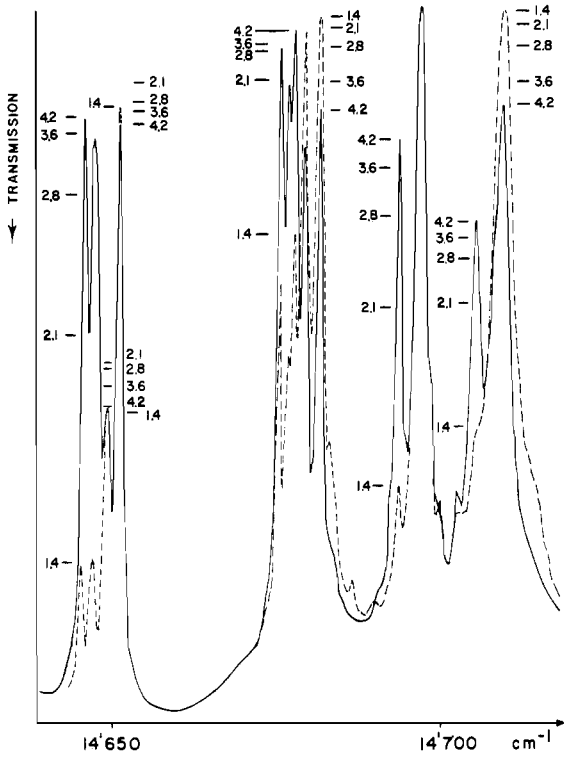

Figure 10. Transmission spectra (X polarization) of bands A–D in $[NH_3]Cl_4 \cdot 4H_2O$ as a function of temperature. Spectra at 4.2 and 1.4 K are given explicitly, and peak heights for intermediate temperatures are indicated.

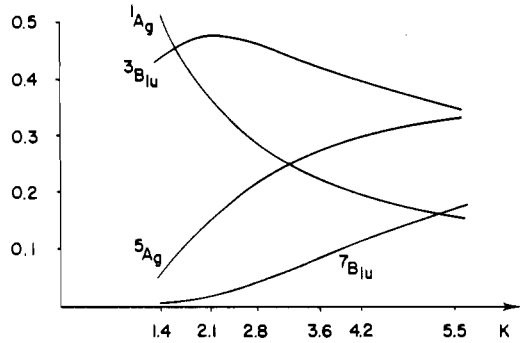

Figure 11. Boltzmann populations of ground-state components in $[NH_3]Cl_4 \cdot 4H_2O$. $J_{ab} = -0.6$ cm^{-1}.

The observed splittings in the bands A, C, and D can be rationalized with the same parameters. The single-ion anisotropy has a sizable rhombic component. This is in agreement with the observation of three components of the spin-allowed $^4A_{2g} \rightarrow {}^4T_{2g}$ transition in $[NH_3]Cl_4 \cdot 4H_2O$.[6]

A similar procedure is used for the analysis of the $[NH_3]Br_4 \cdot 4H_2O$ spectra. The ground-state exchange splittings are even smaller than in $[NH_3]Cl \cdot 4H_2O$, and complementary Zeeman experiments[24] were used to determine the exchange parameter: $J_{ab} = -0.30 \pm 0.15$ cm^{-1}. Zero-field splittings in the excited pair states are of the same order as in $[NH_3]Cl_4 \cdot 4H_2O$. Exact anisotropy parameter values cannot be derived due to the lower resolution of the fine structure.

The next step is the assignment of bands A–H to $^2E_g {}^4A_{2g}$ pair transitions. From the data in Figure 10 and Table VII, partly supplemented by Zeeman measurements,[24] it is possible to determine the spin multiplicities of the final pair states. We thereby assume that the dominant absorption bands correspond to $\Delta S = 0$ and $\Delta S = \pm 1$ transitions according to the mechanisms in section 3.3. The bands A, C, F, and H are thus assigned to $^5\Gamma$ excited states and B, D, E, and G to $^3\Gamma$. Of the highly structured transitions B is the only one strictly obeying the selection rule $\Delta S = \pm 1$, whereas the band systems A and C contain both $\Delta S = 0$ and $\Delta S = \pm 1$ components. According to the theory transitions should be either $\Delta S = 0$ or $\Delta S = \pm 1$ but not both. As in the $[en]Br_4 \cdot 2H_2O$ spectra selection rules based on the idealized C_{2v} single-ion point symmetry are violated. Additional odd-parity potentials of the true C_i point symmetry may contribute to the intensity. Anisotropy effects may also be relatively more important in this case than in $[en]Br_4 \cdot 2H_2O$, because of the smallness of the isotropic exchange. Band system B appears to be free of such complications. It consists of three $^1A_g \rightarrow {}^3\Gamma$ and three $^5A_g \rightarrow {}^3\Gamma$ components, and we assign it to either $^3B_{1u}$ or $^3B_{2u}$, the only allowed $\Delta S = \pm 1$ transitions to triplet states.

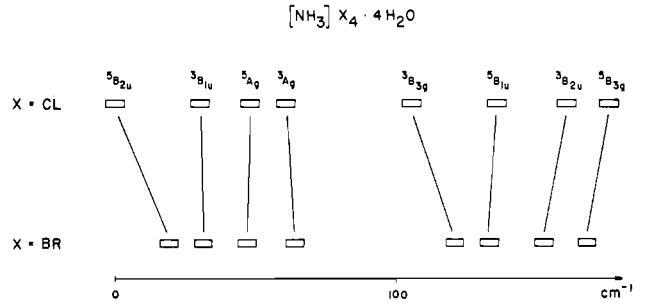

Figure 12. Correlation of observed $^2E_g {}^4A_{2g}$ transitions in $[NH_3]Cl_4 \cdot 4H_2O$ and $[NH_3]Br_4 \cdot 4H_2O$.

With this and the constraints on the exchange parameters (eq 19), which were already used in the interpretation of the $[en]Br_4 \cdot 2H_2O$ spectrum, there remains only one possible assignment of the bands A–H. It is included in Figures 5 and 6, and the resulting exchange parameters are collected in Table VIII. In Figure 12 the splitting of the excited $^2E_g {}^4A_{2g}$ pair states in $[NH_3]Cl_4 \cdot 4H_2O$ is correlated with that in $[NH_3]Br_4 \cdot 4H_2O$. The main difference between the chloride and the bromide lies in the larger J_{12} parameter of the former, whereas J_{33} is about the same for the two components. This can be rationalized (section 5), and the correlation in Figure 12 thus lends further support to our assignments.

5. Discussion

In all the three compounds investigated J_{12} is the dominant antiferromagnetic contribution to J_{ab}. It corresponds to the superexchange resulting from the mutual overlap of the magnetic zx and yz orbitals with the oxygen $p_z = p_X$ orbital. In the $[NH_3]$ salts J_{12} is reduced by a factor of more than 2 compared with that of $[en]Br_4 \cdot 2H_2O$. The ferromagnetic terms J_{11} and J_{13} are also reduced, but to a lesser extent. J_{33}, the direct antiferromagnetic exchange from the overlap of magnetic xy orbitals, is of minor importance; it is slightly larger in the $[NH_3]$ salts than in $[en]Br_4 \cdot 2H_2O$.

These trends can be understood by a comparison with the structural properties of the compounds (Table VIII). The crystal structure of $[en]Br_4 \cdot 2H_2O$ has been determined,[4] but for $[NH_3]Cl_4 \cdot 4H_2O$ and $[NH_3]Br_4 \cdot 4H_2O$ we have to rely on the structure determinations of the isostructural cobalt(III) compounds.[25] The shorter Cr–Cr distance in $[NH_3]$ accounts for the slightly larger value of J_{33}. This is not an important mechanism, however, and we conclude that Cr–Cr distances in the range 2.95–3.04 Å are too long for appreciable direct exchange. The hydrogen position of the hydroxo-bridging ligand appears to be a far more important parameter. In

(24) Decurtins, S., unpublished work.

(25) (a) Prout, C. K. *J. Chem. Soc.* **1962**, 4429. (b) Vannerberg, N. G. *Acta Chem. Scand.* **1963**, *17*, 85.

$[en]Br_4 \cdot 2H_2O$ the hydrogen atom lies more or less in the

plane, whereas in the $[NH_3]$ salts it is displaced out of this plane by an angle of at least 30° but more likely 50–60°.[6] Hydrogen bonding to chloride and bromide ions is responsible for these displacements. The bonding situation of the oxygen atom and thus the superexchange pathway is affected by this. The $p_z = p_X$ oxygen orbital is fully available for π bonding to zx and yz chromium orbitals if the hydrogen position is in the plane. This is the case in $[en]Br_4 \cdot 2H_2O$, where J_{12} and, as a consequence, J_{ab} are large. In the $[NH_3]$ salts the $p_z = p_X$ oxygen orbital is involved in the O–H σ bond and therefore not fully available in the superexchange mechanism through π bonding, thus the reduction of J_{12}, J_{11}, and J_{13}. The further reduction of these superexchange parameters and thus of J_{ab} between $[NH_3]Cl_4 \cdot 4H_2O$ and $[NH_3]Br_4 \cdot 4H_2O$ must be fully attributed to changes of the hydrogen-bonding situation. If there are differences in the framework

between the two salts, they are likely to be the consequence of differences in the O–H···X hydrogen bond. A careful determination of atomic positions by X-ray diffraction will be a very important prerequisite for a quantitative discussion of our results.

Our interpretation of the spectroscopic properties of bis(μ-hydroxo)-bridged chromium(III) dimers differs from that by Henning and co-workers for bis(μ-oxo)-bridged chromium(III) dimers in the $ZnGa_2O_4$ host lattice.[7] The Cr–Cr separation can be estimated from the nearest-neighbor Ga–Ga distance of 2.945 Å in the pure host. This distance is comparable to that in $[NH_3]Cl_4 \cdot 4H_2O$. But in contrast to our conclusions for $[NH_3]$ and [en] Henning et al. postulated a dominant direct-exchange mechanism ($J_{33} = -280$ cm^{-1}) for the chromium dimers in $ZnGa_2O_4$ on the basis of optical spectroscopic data. Because $ZnGa_2O_4$ is cubic, these authors had no possibility to measure the polarizations of the pair absorptions. And due to this lack of polarization information they could not experimentally distinguish between two sets of orbital exchange parameters producing the same energy splitting pattern in ^2E_g $^4A_{2g}$. They were forced to make a choice, and they chose the set that was compatible with the generally accepted direct-exchange mechanism in chromium oxide compounds.[9] Our crystals have the advantage that all the dimers are parallel. As a result we obtain polarized spectral information with respect to the molecular symmetry axes. And it is this type of information that is needed to assign the lowest energy pair transitions in $[en]Br_4 \cdot 2H_2O$ to $^5B_{2u}$ and $^3B_{3g}$ transitions and thus obtain a dominant J_{12} contribution. Our $[NH_3]$ spectra have the additional advantage that a great deal of fine structure is resolved, resulting in an enormous increase of spectral information. We are currently reconsidering the problem of direct exchange vs. superexchange in chromium(III) oxide compounds with bis(μ-oxo) bridging geometries between nearest neighbors.

Acknowledgments. We are indebted to L. Dubicki for very helpful correspondence and to A. Pfeuti for preparative assistance. This work was supported by the Swiss National Science Foundation (Grant No. 2.427.79).

Registry No. $[(en)_2Cr(en)_2]Br_4 \cdot 2H_2O$, 15135-03-2; $[(NH_3)_4Cr(OH)_2Cr(NH_3)_4]Cl_4 \cdot 4H_2O$, 82456-39-1; $[(NH_3)_4Cr(OH)_2Cr(NH_3)_4]Br_4 \cdot 4H_2O$, 82469-00-9.

Contribution from the Department of Inorganic and Physical Chemistry, Indian Institute of Science, Bangalore-560012, India

Cation-Induced Crown Porphyrin Dimers of Oxovanadium(IV)

V. THANABAL and V. KRISHNAN*

Received November 23, 1981

Oxovanadium(IV) porphyrins appended with crown ether (benzo-15-crown-5) at the 5 (mono), the 5 and 10/15 (cis/trans bis), the 5, 10, and 15 (tris), and the 5, 10, 15, and 20 (tetrakis) positions have been synthesized. The cation complexation behavior of these cavity-bearing porphyrins has been studied by using optical aborption and ESR spectral methods. The cations K^+, Cs^+, NH_4^+, and Ba^{2+}, which require two crown ether cavities for complexation, induce dimerization of the porphyrins. The cation-induced dimerization constants for a representative tetrasubstituted porphyrin vary as $K^+ > Ba^{2+} > Cs^+ \sim NH_4^+$, and the relative stabilities of the dimers are dependent on the type of the substitution, tetrakis > tris > cis bis. ESR spectra recorded at a sample temperature of 77 K have low-field components attributed to $\Delta M_s = \pm 2$ transitions, providing further evidence for the existence of dimers in solutions. The eclipsed sandwich dimers have V–V distances in the range 4.70 Å. The relative distributions of oxovanadium crown porphyrins in terms of monomeric and dimeric forms rest on the geometric dispositions of the crown ether appendages.

Introduction

Aggregation of macrocyclic compounds in general, and tetrapyrrole pigments in particular, is one of the properties of significance in biological systems. Central to aggregation, the dimerization process is widespread among porphyrins and their metal derivatives both in solution and in solid state. The formation of dimers in solution is shown to be dependent on concentration[1] while in some cases intentional syntheses of covalently linked dimers have been achieved.[2] In the latter, it is found that variations of interplanar separations can be controlled by a proper choice of linking groups whereas, in the concentration-dependent dimers, the interplanar distances are contrived and specific to the nature of the porphyrins. In our studies in the development of supramolecular entities, having

(1) (a) Blumberg, W. E.; Peisach, J. *J. Biol. Chem.* **1965**, *240*, 870. (b) Pasternack, R. F.; Huber, P. R.; Boyd, P.; Engasser, G.; Francesconi, L.; Gibbs, E.; Fasella, P.; Venturo, G. C.; Hinds, L. deC. *J. Am. Chem. Soc.* **1972**, *94*, 4511. (c) Das, R. R.; Plane, R. A. *J. Inorg. Nucl. Chem.* **1975**, *37*, 147. (d) Das, R. R. *Ibid.* **1975**, *37*, 153. (e) White, W. E.; Plane, R. A. *Bioinorg. Chem.* **1974**, *4*, 21. (f) Boyd, P. D. W.; Smith, T. D. *J. Chem. Soc., Dalton Trans.* **1972**, 839. (g) Boyd, P. D. W.; Smith, T. D.; Price, J. H.; Pilbrow, J. R. *J. Chem. Phys.* **1972**, *56*, 1253.

(2) (a) Schwart, F. P.; Gouterman, M.; Mulijiani, Z.; Dolphin, D. H. *Bioinorg. Chem.* **1972**, *2*, 1. (b) Collman, J. P.; Elliott, C. M.; Helbert, T. R.; Tovrog, B. S. *Proc. Natl. Acad. Sci. U.S.A.* **1977**, *74*, 18. (c) Kagen, N. E.; Mauzerall, D.; Merrifield, R. B. *J. Am. Chem. Soc.* **1977**, *99*, 5484. (d) Chang, C. K.; Kuo, M. S.; Wang, C.-B. *J. Heterocycl. Chem.* **1977**, *14*, 943. (e) Ogoshi; Sugimoto, H.; Yoshida, Z. *Tetrahedron Lett.* **1977**, *169*. (f) Anton, J. A.; Loach, P. A.; Govindjee. *Photochem. Photobiol.* **1978**, *28*, 235. (g) Collman, J. P.; Denisevich, P.; Konai, Y.; Marroco, M.; Koval, C.; Anson, F. C. *J. Am. Chem. Soc.* **1980**, *102*, 6027. (h) Collman, J. P.; Chong, A.; Jameson, G. B.; Oakley, R.; Rose, E.; Schmittou, E. R.; Ibers, J. A. *Ibid.* **1981**, *103*, 516.

0020-1669/82/1321-3606$01.25/0